Engineering Journal issn: 0125-8281

Article

Carbon Dioxide Capture in a Fixed Bed of Coconut Shell Activated Carbon Impregnated With Sodium Hydroxide: Effects of Carbon Pore Texture and Alkali Loading

Suravit Naksusuk[a], **and Chaiyot Tangsathitkulchai**[b,*]

School of Chemical Engineering, Institute of Engineering, Suranaree University of Technology, Nakhon Ratchasima 30000, Thailand
E-mail: [a]suravit_64@hotmail.com, [b]chaiyot@sut.ac.th (Corresponding author)

Abstract. Performance of CO_2 adsorption was investigated in a fixed bed of coconut shell activated carbon impregnated with sodium hydroxide with emphasis on the effect of alkali loading and carbon pore texture. CO_2 adsorption capacity increased with the increase of NaOH loading and passed through a maximum value at the optimum loading of 180 g NaOH/g carbon. This optimum loading appeared to be the same, independent of the surface area of activated carbon in the range of 766-1052 m^2/g. A pore blocking phenomenon was proposed to account for the effect of alkali loading on the CO_2 adsorption behavior. Empirical equations were also developed to correlate the breakthrough time, the adsorption capacity at breakthrough time and the equilibrium adsorption capacity with alkali loading and surface area of activated carbon. The breakthrough equation based on the LDF model was found to describe the experimental breakthrough data reasonably well. The transport of CO_2 molecules in the pore structure of activated carbon to the adsorption sites is governed by the mechanism of surface diffusion and the surface diffusivity is about two orders of magnitude larger than the pore diffusivity.

Keywords: Activated carbon, adsorption, breakthrough curves, CO_2 adsorption, alkali impregnation.

ENGINEERING JOURNAL Volume 23 Issue 4
Received 6 November 2018
Accepted 26 April 2019
Published 8 August 2019
Online at http://www.engj.org/
DOI:10.4186/ej.2019.23.4.29

DOI:10.4186/ej.2019.23.4.29

1. Introduction

CO_2 generated from power plants burning fossil fuels and large industrial sectors has posed a serious problem and concern to global warming and climate change [1,2]. Worldwide, power generation alone emits nearly 10 billion tons of CO_2 annually, accounting for about 25% of total CO_2 emission [3]. As a result, there is an urgent need to be able to control the level of CO_2 being released into the atmosphere from those anthropogenic sources. Current technologies dealing with CO_2 removal have been achieved through the process of carbon capture and storage (CCS), consisting of three consecutive steps of carbon capture, transportation to the storage site and depositing in deep geological formations or in the form of mineral carbonates [4]. The capture of CO_2 is achieved by pre-combustion capture, post-combustion capture and oxy-fuel combustion. Of these processes, the post-combustion capture is the most preferred choice due to the ease of retrofitting the existing power plants without affecting the overall process performance [5].

With regard to the post-combustion process, the separation of CO_2 from flue gas by absorption with liquid solvents such as monoethanolamine (MEA) and diethanolamine (DEA) is the most mature technology. However, despite the high separation efficiency of the chemical absorption system, it has a number of inherent drawbacks, for example, amine degradation that results in solvent loss and the generation of many toxic substances, high corrosiveness of the solvents and high energy consumption for solvent recovery [6,7]. Due to these limitations, adsorption technology has emerged as a promising alternative for CO_2 removal from flue gas. It offers many advantages including, low manufacturing cost, high thermal stability, high adsorption capacity, low energy requirement, and low sorbent regeneration cost [8-10]. Among the various available adsorbents for CO_2 capture, the use of activated carbon is quite attractive. It has several desirable properties such as flexibility of controlling pore size distribution during preparation, large surface area, large micropore volume for effective CO_2 adsorption, reasonably high pellet strength, fast regeneration for repeated usage, insensitivity to moisture due to surface hydrophobicity and capability of surface chemical modification for increased sorption selectivity [11]. There are a number of investigations on CO_2 capture by physically- and chemically-activated carbon prepared from various biomass waste [12-14]. The equilibrium adsorption capacity for CO_2 was reported to be in the range of 2-5 mmol/g at 25^{o}C and decrease with increasing the adsorption temperature, hence indicating the physical adsorption between adsorbent and adsorbate molecules.

The adsorption capacity of CO_2 from flue gas can be further increased by increasing the affinity and selectivity of CO_2 toward the carbon surface. Since CO_2 is an acid gas, the creation of basic sites onto the surface of activated carbon will help increase the adsorption selectivity by acid-base interaction [15]. The most commonly used method of introducing the basic sites is by wet impregnating the activated carbon with an alkali solution such as ethanolamine, KOH and NaOH [16-18]. However, in contrast to the CO_2 adsorption with the unmodified activated carbon which requires a high proportion of microporosity, mesoporous carbon is more appropriate for the impregnation process to prevent the blocking of pore structure at high alkali loadings [5].

In general, adsorption study can be performed in batch mode or continuous mode. For a batch operation, information on both equilibrium (isotherm data) and kinetics (data on how fast the adsorbate molecules transport to the adsorption sites) are of prime interest. For a continuous operation, adsorption is often performed in a fixed bed of solid adsorbent due to its wide spread applications in industries. The present work is therefore focused on studying the capture of CO_2 from a gas mixture of CO_2 and N_2 whose composition simulates that of the flue gas. Adsorption experiments were carried out in a fixed bed column and the adsorbent particles used were coconut shell activated carbon impregnated with a sodium hydroxide solution. Sodium hydroxide was employed as an impregnant because of its low cost and easy availability. Two major parameters, which directly affect the number of adsorption sites and hence the adsorption performance, including pore texture of the test carbon and the amount of alkali loading, were investigated. A model was proposed to explain the role of NaOH loading on the adsorption efficiency of carbon dioxide. In addition, empirical correlations were also proposed for the adsorption capacity of CO_2 as functions of NaOH loading and surface area of the tested activated carbons.

2. Theory

2.1. Adsorption Performance of a Fixed Bed

The adsorption performance of an adsorbate in a fixed bed of adsorbent particles can be assessed by following the response of the exit concentration of the adsorbate as a function of time. The collected information presented as a plot of the ratio of the outlet and inlet adsorbate concentration (C/C_o) versus time is called the breakthrough curve which has a characteristic of a S-shaped curve. The steepness (slope) and position on the time scale reflect the adsorption behavior of adsorbate inside the adsorbent bed. A steeper slope indicates the lowering of internal mass transfer resistance for transporting the adsorbate to the adsorption sites, while the shifting of the curve to a higher value of time scale signifies a strong affinity between the adsorbent and adsorbate molecules. Both characteristics imply the increased adsorption capacity of the adsorbate. The time at which $C/C_o = 0.05$ is termed the breakthrough time (t_B), which is the time that the adsorption operation is to be interrupted and the regeneration of the solid adsorbent is required. The time at which $C/C_o = 0.95$, where the bed becomes fully exhausted, is called the equilibrium time (t_E). The adsorption capacity of adsorbate at t_B and t_E can then be calculated from the breakthrough data by the following equations [16]

$$q_B = (\frac{C_0 Q}{W})\int_0^{t_B}[\frac{1-C}{C_0}]dt \tag{1}$$

$$q_E = (\frac{C_0 Q}{W})\int_0^{t_E}[\frac{1-C}{C_0}]dt \tag{2}$$

where C and C_o = outlet and inlet concentration of adsorbate, respectively, Q = volume flow rate of the feed gas and W = weight of adsorbent. The integral terms in Eqs. (1) and (2) can be estimated from the areas above the breakthrough curve at t_B and t_E, respectively.

2.2. Breakthrough Model

A mathematical equation describing the breakthrough curve can be derived by performing a mass balance on a single adsorbate over a differential length of the adsorbent bed under an isothermal condition [19]. The resulting equation obtained reads

$$-D_Z\frac{\partial^2 C}{\partial z^2} + u\frac{\partial C}{\partial z} + \frac{\partial C}{\partial t} + \frac{(1-\varepsilon_b)}{\varepsilon_b}\frac{\partial \bar{q}}{\partial t} = 0 \tag{3}$$

and

$$\bar{q} = \frac{3}{R_p^3}\int_0^{R_p} qr^2 dr \tag{4}$$

where q = adsorbed-phase concentration, D_z = axial dispersion coefficient, C = adsorbate concentration in the fluid phase, u = interstitial gas velocity, R_p = radius of an adsorbent particle, ε_b = bed porosity, z = distance along the bed and t = time.

Equations (3) and (4) can be solved based on the complexity of the model assumptions, for example, isothermal or adiabatic operations, trace or high concentration of adsorbate, type of adsorption isotherms (linear or curved) to arrive at the concentration profile of the adsorbate inside the adsorption bed as a function of time. To obtain the breakthrough equation (C/C_o vs. t), the axial distance (z) in the concentration profile equation is just replaced by the bed length (L_B).

The simplest model to obtain the breakthrough equation is based on the concept of the linear driving force model (LDF) [20] which assumes that the effect of axial dispersion is negligible, the adsorption isotherm is linear and the rate of adsorption can be represented by the following linear rate equation.

DOI:10.4186/ej.2019.23.4.29

$$\frac{\partial \bar{q}}{\partial t} = k_p(q^* - \bar{q}) = k_p K(C - C^*) \tag{5}$$

where k_p is the particle mass transfer coefficient, K is the Henry constant of the linear isotherm, q* is the adsorbed - phase concentration that is in equilibrium with the bulk phase concentration (C) and C* is the bulk-phase concentration that is in equilibrium with the average adsorbed-phase concentration ($\bar{q}$).

The breakthrough equation derived from the LDF theory is referred to as the Klinkenberg's model [21]. The approximate equation for a long bed is given by

$$\frac{C}{C_0} = \frac{1}{2}[1 + erf(\sqrt{\tau} - \sqrt{\xi} + \frac{1}{8\sqrt{\tau}} + \frac{1}{8\sqrt{\xi}})](error < 0.6\% \; for \; \xi > 2.0) \tag{6}$$

where $\xi = k_p K L_B(1-\varepsilon_b)/u\varepsilon_b$ and $\tau = k_p[t-(L_B/u)]$

The term k_pK in Eq. 5 is related to the external and internal mass transfer resistances as characterized by the film mass transfer coefficient (k_c) and the effective pore diffusivity (D_e), respectively, as follows [19]

$$\frac{1}{k_p K} = \frac{R_p}{3k_c} + \frac{R_p^2}{15D_e} \tag{7}$$

where R_p is the radius of the adsorbent particle.

The film mass transfer coefficient (k_c) can be estimated from the correlation of Sherwood number (N_{Sh}) with correction for axial dispersion as proposed by Wakao and Funazkri [22]. The equation reads

$$N_{Sh} = \frac{k_c d_p}{D_m} = 2 + 1.1(\frac{d_p G}{\mu})^{0.6}(\frac{\mu}{\rho D_m})^{1/3} \tag{8}$$

where d_p = particle diameter, D_m = molecular diffusivity of the diffusing species, G = mass velocity of fluid, μ = fluid viscosity and ϱ = fluid density.

The molecular diffusivity of CO_2 in a binary mixture of CO_2 and N_2 is determined from the Chapman-Enskog equation [23] and has a value of 1.74×10^{-5} m^2/s. The film mass transfer coefficient of CO_2 (k_c) calculated from Eq. (8) is equal to 0.0278 m/s.

3. Material and Method

3.1. Raw Materials

The activated carbon used in this study is a commercial activated carbon produced from coconut shell by steam activation and supplied by C. Gigantic Carbon Co., Ltd., Nakhon Ratchasima, Thailand. It has an average particle size of 1.29 mm (14x16 mesh screen size). Two types of activated carbon (designated as AC1 and AC2) having different pore structures were employed in the present work. The BET surface area and total pore volume of AC1 and AC2 are 766 m^2/g and 0.387 cm^3/g, and 1,052 m^2/g and 0.547 cm^3/g, respectively. Carbon dioxide gas and nitrogen gas of high purity (99.99%) being used for the adsorption study were purchased from Linde Thailand. Sodium hydroxide pellets (AR grade) was purchased from Carlo Erba Reagents.

3.2. Alkali Impregnation

Alkali impregnated activated carbon was prepared by mixing 50 g of activated carbon, corresponding to a bulk volume of 110 cm^3 and void volume of 45 cm^3, with 180 cm^3 of NaOH solution of the desired concentration (3-15 wt% NaOH). Next, the mixture was shaken in a water bath at room temperature using

the shaking speed of 180 rpm for 90 min to reach equilibrium. The whole sample was then dried in an electric oven at 110°C for 48 h. Each impregnated carbon was given a sample name by the type of activated carbon (AC1 or AC2) followed by the weight % of NaOH solution used for the impregnation. For example, sample AC1-5 indicates activated carbon AC1 which was impregnated with 5 wt% NaOH solution.

3.3. Pore Characterization of Activated Carbons

Porous properties of the original and alkali impregnated activated carbons were determined from the N_2 adsorption isotherms measured at -196°C (77K) using the surface area analyzer (ASAP2010, Micromeritics, US). Specific surface area of each activated carbon sample was calculated from the derived N_2 isotherms employing the BET equation [24]. The micropore volume was computed from the t-plot method [25]. The total pore volume was determined from the amount of gas adsorbed at the relative gas pressure (P/P^o) of 0.98, and converted this number to the volume of N_2 in liquid state. The average pore diameter was calculated from the equation 4V/A based on the assumption of cylindrical pore shape, where V and A represent the total pore volume and BET surface area, respectively.

3.4. Fixed-bed Adsorption of CO_2

The study of CO_2 adsorption in a fixed bed of virgin and alkali impregnated activated carbon was carried out at atmospheric pressure in a clear acrylic column of 1 cm in diameter and 60 cm in height. Figure 1 shows the experimental set up for CO_2 adsorption experiments. The adsorption temperature was fixed at 35°C for all experimental runs by circulating water from a temperature-controlled water bath through the column jacket. The column was first purged with nitrogen gas flowing at the rate of 100 cm^3/min for 15 min. After that, activated carbon was loaded into the column to the desired height. Next, nitrogen and carbon dioxide were allowed to flow from the supply tanks and mixed thoroughly along a long pipe section and passed through a by-pass line at the pre-calculated flow rates (measured with two separate rotameters for each gas) to give the gas mixture composition of 13 vol% CO_2 (an average CO_2 concentration in the flue gas burning a solid fuel). A portable gas analyzer (BIOGAS 5000, Geotech, UK) was used to check for the required inlet CO_2 concentration. Now, the feed gas mixture was admitted into the adsorption column and the timing was started. The exit concentration of CO_2 was recorded as a function of time using the gas analyzer until the measured concentration approached the inlet CO_2 concentration. Table 1 summarizes the experimental conditions used for the adsorption study.

Table 1. Experimental conditions for CO_2 adsorption study

Conditions	Values
NaOH concn. for impregnation (wt%)	0-15
Surface area of activated carbon (m^2/g)	766, 1052
%CO_2 in the feed gas (vol%)	13
Amount of activated carbon (g)	10
Bed height (cm)	28.2
Gas superficial velocity (m/min)	3.03
Temperature (°C)	35

DOI:10.4186/ej.2019.23.4.29

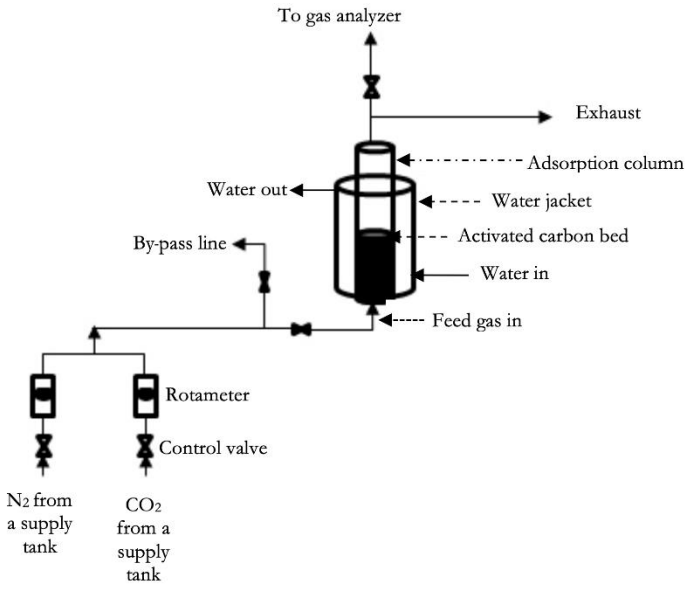

Fig. 1. Schematic of experimental set-up for CO_2 adsorption study.

4. Results and Discussion

4.1. Pore Structure of Activated Carbons

Figure 2 shows typical nitrogen adsorption-desorption isotherms of the tested activated carbons. All isotherms show Type I isotherm according to the IUPAC classification [26], typified by a sharp increase of the amount adsorbed at low pressures and followed by a plateau region at higher pressures. This type of isotherm indicates that the original activated carbons (AC1 and AC2) prepared from coconut shell contain mostly micropores (pore size smaller than 2 nm) (see Table 2) and the amount of N_2 adsorbed by AC2 is higher than that of AC1, thus indicating larger surface area and pore volume of the AC2 sample.

The N_2 isotherms in Fig. 2 also shows small hysteresis loops notably for the original AC1 and AC2, indicating the existence of some mesopores which was found to possess about 17.8 and 28.2 % of the total pore volume for AC1 and AC2, respectively (see Table 2). It is also observed that the size of hysteresis loop tends to decrease as the NaOH loading is increased, caused by the consequent decrease of the average pore size.

Table 2 lists the porous properties of the original and alkali modified activated carbons. Both the surface area and pore volume tend to decrease as the amount of NaOH depositing in the pores is increased. About a fivefold increase of NaOH loading from 0-540 mg NaOH/g carbon lowers the surface area of AC1 and AC2 by 43.5% and 51.1%, respectively. The continued decrease in surface area with increasing NaOH loading signifies the decreasing amount of N_2 adsorption on the internal surface of activated carbon, as seen from Fig. 2. This result of lowering in surface area is possibly caused by the effect of pore restriction whereby the volume of pore space starts to decline with increasing amount of deposited layer of NaOH molecules inside the pores, giving less area for N_2 adsorption to occur. At a very high NaOH loading, the pores will be completely blocked, thus preventing the diffusion of N_2 to the inner adsorption sites. It is also noted from Table 2 that there is a slight decrease in the average pore size with the increase of NaOH loading.

Table 2. Porous properties of original and NaOH impregnated activated carbons.

Samples	%NaOH solution (wt%)	NaOH loading (mg/g)	BET surface area (m2/g)	Micropore volume (cm^3/g)	Mesopore volume (cm^3/g)	Total pore volume (cm^3/g)	Average pore diameter (nm)
AC1	0	0	766	0.318 (82.2%)	0.069 (17.8%)	0.387	2.02
AC1-3	3	108	663	0.279 (84.5%)	0.051 (15.5%)	0.330	1.99
AC1-5	5	180	593	0.249 (83.8%)	0.048 (16.2%)	0.297	2.00
AC1-7.5	7.5	270	529	0.219 (82.6%)	0.046 (17.4%)	0.265	2.00
AC1-10	10	360	527	0.218 (80.7%)	0.042 (19.3%)	0.270	2.05
AC1-15	15	540	433	0.183 (85.1%)	0.052 (14.9%)	0.215	1.99
AC2	0	0	1052	0.393 (71.8%)	0.154 (28.2%)	0.547	2.08
AC2-3	3	108	841	0.330 (78.6%)	0.090 (21.4%)	0.420	2.03
AC2-5	5	180	827	0.319 (77.6%)	0.092 (22.4%)	0.411	2.03
AC2-7.5	7.5	270	750	0.297 (80.3%)	0.073 (19.7%)	0.370	2.01
AC2-10	10	360	659	0.264 (80.2%)	0.065 (19.8%)	0.329	2.00
AC2-15	15	540	514	0.198 (76.4%)	0.061 (23.6%)	0.259	2.01

DOI:10.4186/ej.2019.23.4.29

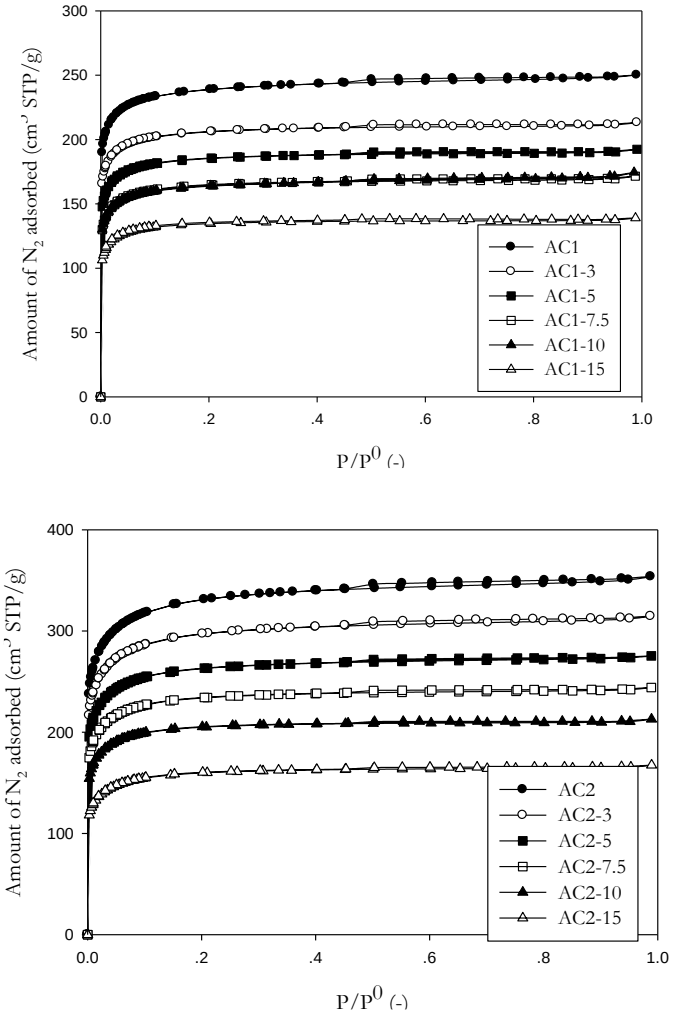

Fig. 2. N_2 adsorption isotherm of the original and NaOH impregnated activated carbons at -196°C (77K).

4.2. Adsorption Performance

The effects of surface area and NaOH loading on the breakthrough curves are illustrated in Figs. 3 and 4. It is clear that both variables exert a strong influence on the breakthrough time (t_B) and equilibrium time (t_E). However, there is virtually no effect of surface area and alkali loading on the slope of the breakthrough curves. In principle, the slope should consistently decrease with increasing alkali loading, caused by the consequent increase of mass transfer resistance that retards the transport of adsorbate molecules to the adsorption sites.

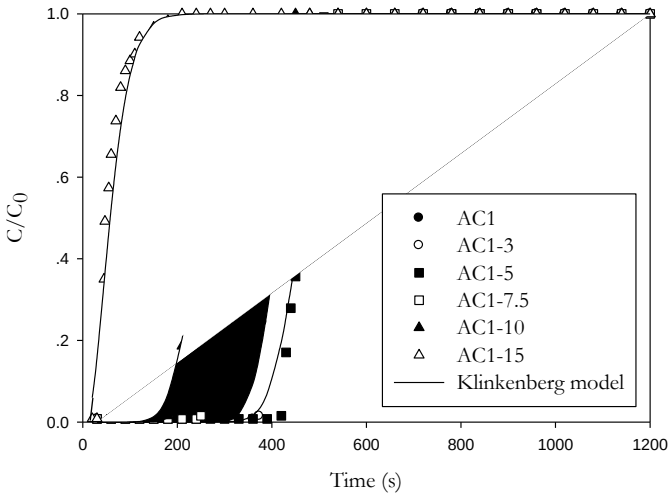

Fig. 3. Breakthrough curves for CO_2 adsorption in a fixed bed of AC1 activated carbon impregnated with NaOH.

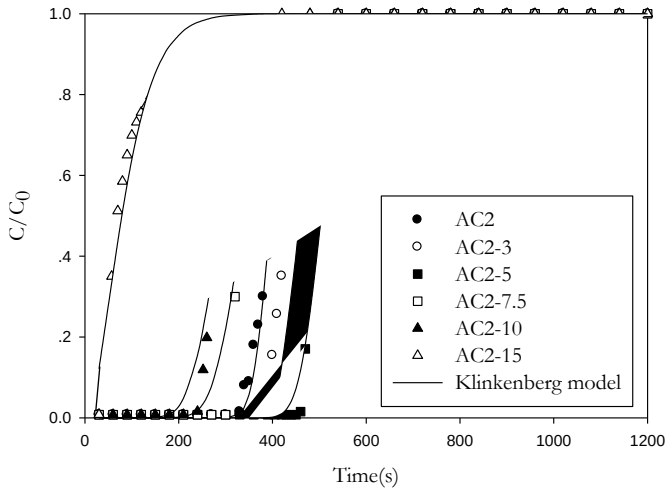

Fig. 4. Breakthrough curves for CO_2 adsorption in a fixed bed of AC2 activated carbon impregnated with NaOH.

Figures 5, 6 and 7 show the effects of NaOH loading and carbon surface area on the breakthrough time (t_B), the adsorption capacity at breakthrough time (q_B) and the adsorption capacity at equilibrium time (q_E), respectively. All curves show similar patterns in that the value of each parameter increases with the increase of NaOH loading and passes through a maximum value at an optimum NaOH loading. The AC2 sample which has a larger surface area than AC1 gives correspondingly higher values of t_B, q_B and q_E at the same alkali loading. The optimum loading occurs at the value of 180 mg NaOH/g carbon, corresponding to the 5 wt% NaOH solution, irrespective of the type of activated carbon at least for the surface area in the range from 766 to 1052 m^2/g. The amount of CO_2 adsorbed at the breakthrough time for AC1 with optimum alkali loading is 43% higher than that of the unmodified AC1 (17.5 vs 25.0 mg/g), while for AC2 the increase is around 40% (19.3 vs 26.8 mg/g).

The increasing-decreasing characteristic of t_B, q_B and q_E with increasing alkali loading is associated with the competing effect of mass transport and adsorption process. At a low alkali loading, the diffusion rate of CO_2 is unaffected by the presence of NaOH inside the pores. Therefore, the amount of CO_2 adsorbed by the acid-base interaction is primarily determined by the number of active sites, leading to an increased adsorption capacity with an increasing NaOH loading. However, as the alkali loading is continually increased

to the point at which pore restriction (the decreasing of mean pore size) comes into effect, the mass transport will dictate the overall adsorption process and thus the adsorption rate drops significantly at a high alkali loading.

Figure 8 shows SEM images of activated carbons (AC2 samples) impregnated with five different concentrations of NaOH solution (0, 3, 5, 8 and 15 wt%). There is clear evidence of NaOH particles dispersing on the activated carbon surface after the impregnation process. The number of residing particles appears to increase progressively with the increase of NaOH solution used for the impregnation. The width of pore mouth tends to get narrower as the NaOH loading is increased. At the optimum concentration of 5 wt% NaOH that gives the maximum adsorbed amount of CO_2, some pore openings can still be observed. However, at higher concentration levels, the pore entrance is completely covered by the deposited layer of NaOH particles. These images evidently support the role of pore restriction effect on the adsorption capacity of CO_2 by the alkali impregnated carbon, as previously discussed.

To analyze the pore blocking effect further, an attempt is made here to estimate the critical pore size that the drop in the adsorption capacity is observed. A pore in activated carbon adsorbent is assumed to be a cylindrical tube having an average diameter d_p and length L. Hence, the pore volume is

$$V_T = \frac{\pi}{4} d_p^2 L \tag{9}$$

At the optimum NaOH loading that gives the maximum adsorbed amount of CO_2, the volume of a NaOH deposited layer (V_{op}) which reduces the pore diameter from d_p to the critical pore diameter (d_c) can be written as

$$V_{op} = \frac{\pi}{4} (d_p^2 - d_c^2) L \tag{10}$$

Eliminating L from Eqs. (9) and (10) yields

$$d_c = d_p [1 - \frac{V_{op}}{V_T}]^{1/2} \tag{11}$$

As an example of the calculation, consider the activated carbon AC1. For this case, we have V_T = 0.387 cm^3/g, the optimal alkali loading is 180 mg NaOH/g carbon, the solid density of NaOH is 2.165 g/cm^3 and the mean pore diameter of AC1 (d_p) is 20.2 A^o (2.02 nm). Therefore, we obtain $V_{op} = 180 \times 10^{-3}/2.165$ = 0.0831 cm^3/g.

Substituting V_T and V_{op} into Eq. (11) gives d_c = 17.90 A^o (1.79 nm). Thus, when the pore size of AC1 is reduced to a size smaller than 1.79 nm due to the increasing deposition of NaOH inside the pores, the adsorption capacity will start to fall. A similar calculation for AC2 gives a slightly larger critical pore size of 19.10A^o (1.91nm).

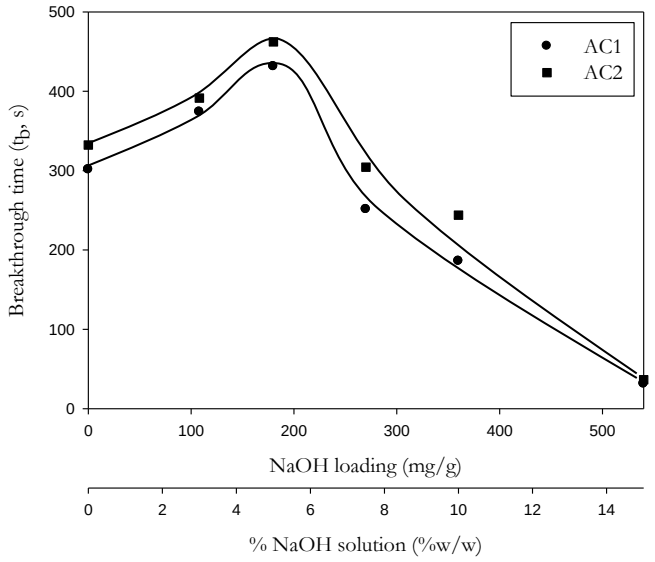

Fig. 5. Effects of NaOH loading and carbon surface area on the breakthrough time (t_b) at 35 °C.

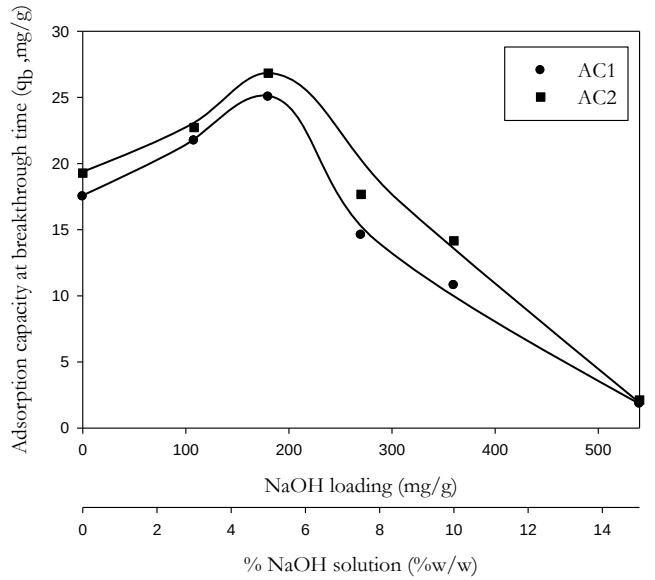

Fig. 6. Effects of NaOH loading and carbon surface area on the CO_2 adsorption capacity at breakthrough time at 35 °C.

Empirical expressions of polynomial type were proposed for correlating t_B, q_B and q_E as functions of activated carbon surface area and NaOH loading, giving the results as follows

$$t_B \text{ (sec)} = 330 - 4.9\text{x}10^{-1}X_1 - 10^{-3}X_2 - 2.55\text{x}10^{-3}X_1^2 + 1.16\text{x}10^{-3}X_1X_2 \text{ , } R^2 = 0.86, \text{ SEE} = 0.156 \quad (12)$$

$$q_B \text{ (mg/g)} = 19.0 - 2.77\text{x}10^{-2}X_1 - 1.48\text{x}10^{-4}X_1^2 + 6.7\text{x}10^{-5}X_1X_2 \text{ , } R^2 = 0.86, \text{ SEE} = 0.307 \quad (13)$$

$$q_E \text{(mg/g)} = 14.3 - 4.4\text{x}10^{-3}X_1 + 8.4\text{x}10^{-3}X_2 - 1.39\text{x}10^{-4}X_1^2 + 4\text{x}10^{-5}X_1X_2 \text{ , } R^2 = 0.83, \text{ SEE} = 0.168 \quad (14)$$

where X_1 = surface area of unmodified activated carbon in the range from 766 - 1052 m^2/g
X_2 = NaOH loading in the range from 0 - 540 mg/g
R^2 = regression coefficient

SEE = overall standard error of estimate, defined as

$$SEE = \sqrt{\sum_{i=1}^{n} [(x_{i,\exp} - x_{i,cal}) / x_{i,cal}]^2 / (N-2)} \quad (15)$$

$x_{i,exp}$ and $x_{i,cal}$ = experimental and calculated value of each respective parameter, respectively
N = number of data points.

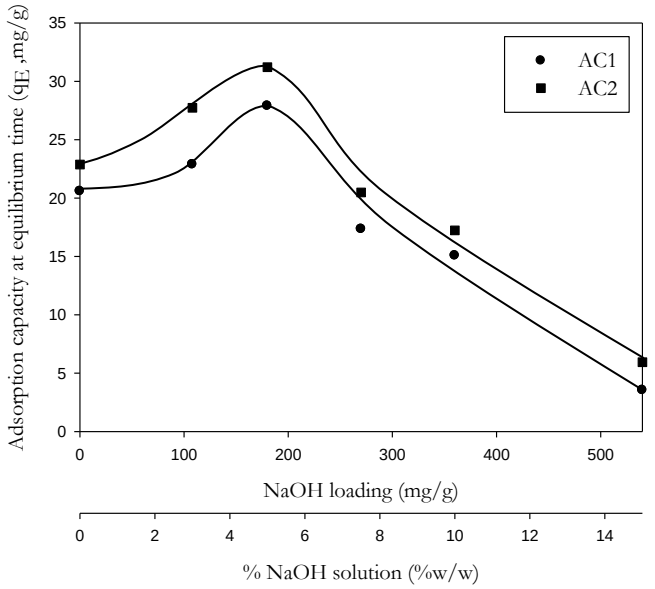

Fig. 7. Effects of NaOH loading and carbon surface area on the CO_2 adsorption capacity at equilibrium time at 35 ^oC

Table 3 summarizes the previous works on CO_2 adsorption by various alkali impregnated adsorbents in a fixed bed operation. It is observed that the alkali impregnated adsorbents can increase the CO_2 adsorption capacity by 25 to 300%, as compared to the use of untreated adsorbents. Diethanolamine-impregnated carbons appear to give higher selectivity toward CO_2 capture than with sodium hydroxide impregnation under comparable adsorption conditions. It is also interesting to note that adsorption of CO_2 at a relatively high temperature of 75^oC by amine impregnated titanium oxides gives a substantial increase of adsorption capacity. Other operating variables such as gas-solid contact time, adsorbent pore structure and feed compositions will also have a direct effect on the overall adsorption efficiency. A comparison was made on the adsorption capacity of CO_2 from the present study and the work of Tan et al. [18] using coconut-shell activated carbon impregnated with NaOH. It was discovered that the alkali impregnated carbon was able to increase the amount of CO_2 adsorbed by 41% and 56% for this work and the work of Tan et al., respectively, although the gas velocity of the latter was much higher.

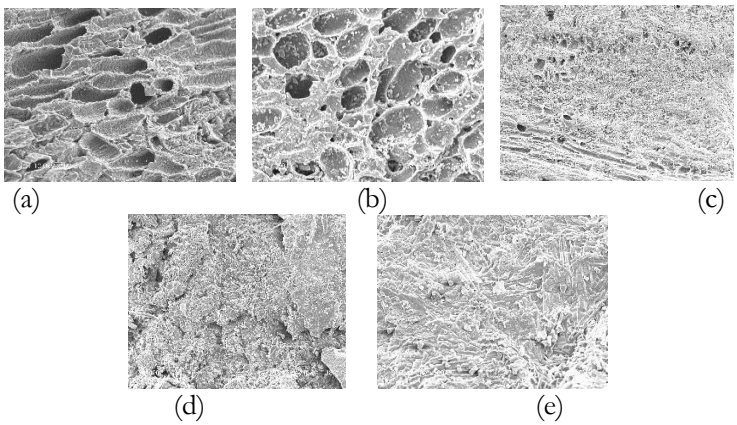

Fig. 8. SEM images of activated carbon (AC2) impregnated with different concentrations of NaOH solution, (a) 0 wt% NaOH, (b) 3wt%, (c) 5wt%, (c) 8wt%, and (e)15wt%.

4.3. Breakthrough Equation

The breakthrough model of Klinkenberg (Eq. (6)) was tested against the experimental breakthrough data to check for the validity of the model and the comparison is shown plotted in Figs. 3 and 4. The accuracy of model fitting is satisfactory for $C/C_o \leq 0.80$. However, there is a tendency for the model to over-predict the experimental results for C/C_o larger than 0.80. Since the practical operating time of a fixed-bed adsorption system is generally the breakthrough time at which C/C_o equals 0.05, the validity of the Klinkenberg's model for the adsorption system studied in this work is acceptable for its application in the design and scaling up for the adsorption of CO_2 by the impregnated activated carbons in a fixed-bed adsorber. The two model parameters, the particle-mass transfer coefficient (k_p) of the LDF equation and the Henry's constant of the linear isotherm (K), were estimated by applying a non-linear regression fitting to minimize the sum of squared errors (SSE) between the experimental and calculated breakthrough data. The effects of NaOH loading and carbon surface area on K and k_p are depicted in Fig. 9 and Fig. 10, respectively. As Fig. 9 shows, the variation of K value with respect to the changes of carbon surface area and NaOH loading follows the same trend as that of the adsorption capacity in Figs. 6 and 7. Since the Henry's constant K is a parameter that determines the affinity between the adsorbent and adsorbate molecules, this result indicates that the adsorbed amount of CO_2 is determined by the number of CO_2 molecules that are transported to the available adsorption sites. In other words, the presence of varying amount of NaOH inside the pores has a direct bearing on the mass transfer resistance (the pore restriction effect) or diffusion rate of the adsorbate molecules, and hence the adsorption capacity of CO_2.

Figure 10 shows that k_p for each activated carbon decreases gradually with the increase of NaOH loading up to the value of about 180 mg/g. It is interesting to note that the loading of 180 mg/g coincides with the optimum loading for maximum adsorption capacity, as reported earlier. At higher loadings from 180 to 270 mg/g, k_p drops sharply with an increasing loading and then falls almost linearly at loadings higher than 270 mg/g. It is logical for k_p to approach zero at a very high loading for each activated carbon at which condition the pore is completely filled by the NaOH impregnant. This maximum NaOH loading can be roughly estimated by extrapolating the linear plot between the total pore volume of activated carbon and loading to intersect the X-axis, as demonstrated in Fig. 11. It was found that the maximum NaOH loading for AC1 and AC2 are 1,210 and 1,484 mg/g, corresponding to NaOH concentration of 33.6 and 41.2 wt%, respectively. It is also noted that k_p of AC2 is larger than that of AC1 for all loadings, but the difference becomes less as the loading is progressively increasing. At relatively low NaOH loading, the larger pore volume of AC2 would allow the transport of CO_2 to the adsorption sites at a much faster rate. However, at higher loadings this advantage is offset by the increasing effect of pore blocking that slows down the overall adsorption process.

Table 3. Typical adsorption capacity of CO_2 in a fixed bed of alkali impregnated adsorbents.

Adsorbent	Column dia. (cm)	Surface area AC (m^2/g)	Bed ht. (cm)	CO_2 concn. (feed) (vol%)	Temp. (^oC)	Gas veloc. (m/s)	Adsorption capacity (mg/g)		Ref.
							Original	Impregd.	
1.NaOH impregnated coconut shell AC	1.0	1052	28.2	13	35	0.033	22.8	32.1	This work
2. Diethanol amine impregnated palm shell AC	2.0	800	60	40	40	10.6	75.0	92.8	[27]
3. Diethanol amine functionalized waste tea AC	1.1	-	10	10	30	0.05	33.6	53.6	[28]
4. NaOH impregnated coconut shell AC	1.1	787	20	20	35	1.8	17.5	27.3	[18]
5. Diethanol amine functionalized activated alumina beads	1.1	205	5	10	35	0.02	-	55	[29]
6. Palm shell AC impregnated with sterically hindered amine	2.0	822	10	30	40	3.2	37.1	64	[30]
7. Amine impregnated titanium oxides	0.6	930	2	10	75	0.02	20.0	91.5	[31]
8. NaOH modified activated alumina	1.1	207	5	15	35	0.02	19.6	51.9	[32]

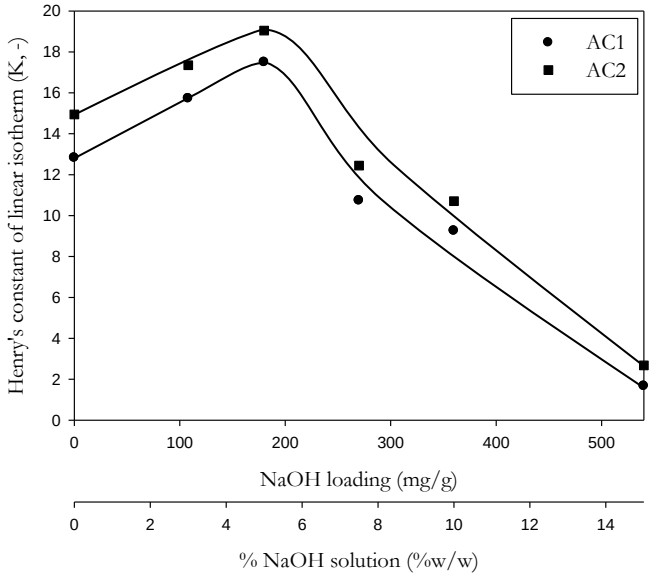

Fig. 9. Effects of NaOH loading and carbon surface area on Henry's constant of linear isotherm at 35 °C.

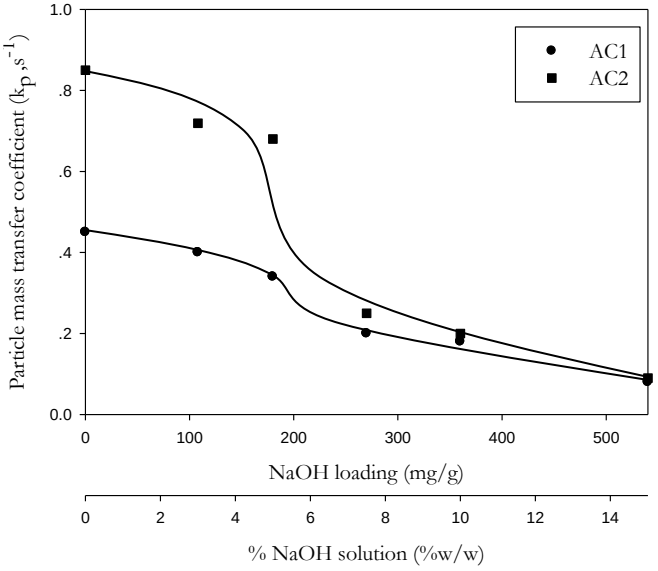

Fig. 10. Effects of NaOH loading and carbon surface area on particle mass transfer coefficient at 35 °C.

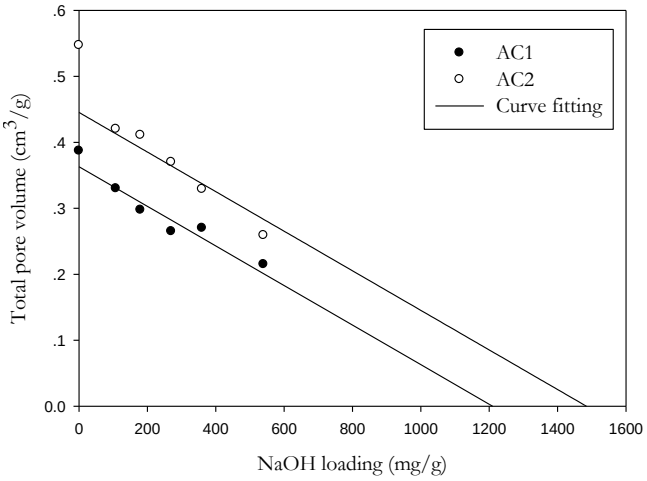

Fig. 11. Variation of total pore volume with NaOH loading for activated carbon AC1 and AC2.

There are two expressions that can be used to arrive at the rate of adsorption ($\partial q / \partial t$) by a porous adsorbent. The first equation is the linear driving force model characterized by the particle mass transfer coefficient (k_p), as shown in Eq. (5). Another equation is derived from the mass balance equation performed on an adsorbate inside a spherical adsorbent, that is,

$$\frac{\partial q}{\partial t} = \frac{D_e}{r^2}\frac{\partial}{\partial r}[\frac{r^2 \partial q}{\partial r}] \tag{16}$$

where D_e is the effective diffusivity that characterizes the diffusive flux of an adsorbate inside the particle and q is the adsorbed-phase concentration. Both D_e and k_p are related according to Eq. (7), as shown previously.

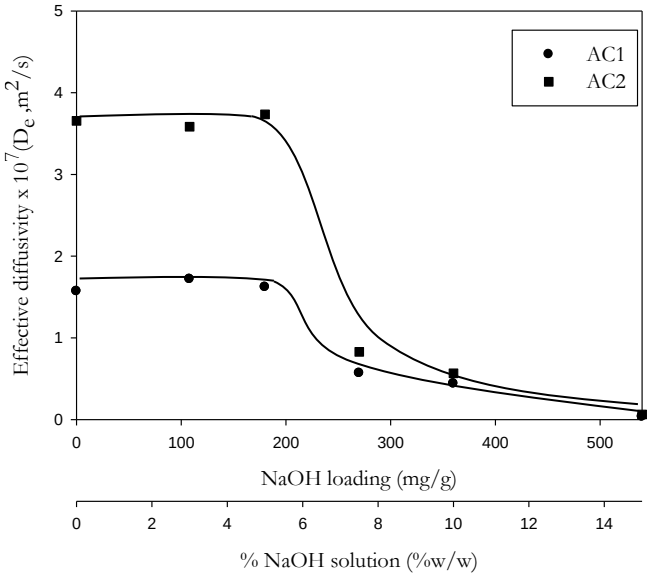

Fig. 12. Effects of NaOH loading and carbon surface area on the effective pore diffusivity (D_e) at 35 °C.

The effect of NaOH loading and surface area of the adsorbents on D_e is shown in Fig. 12. The variation trend of D_e resembles that of k_p in Fig. 10, except that D_e remains relatively constant for loading below the critical loading of 180 mg NaOH/g carbon. This indicates that the increased deposition of NaOH has virtually no effect on the transport flux through the internal pores. Also, in this region AC2 shows a greater diffusivity than that of the AC1 carbon ($3.8x10^{-7}$ vs. $1.57x10^{-7}$ m^2/s), due principally to its larger pore volume and pore size. Again, at a very high alkali loading the transport flux of adsorbate to the adsorption sites will drop dramatically, causing the effective diffusivity to approach zero.

It has been reported by a number of investigators that the fixed-bed adsorption of CO_2 on the surface of alkali impregnated activated carbon at temperatures lower than 40°C involves the physical interaction forces [18, 28, 29, 32], as demonstrated by the decreased amount of CO_2 adsorption with an increasing adsorption temperature. On the contrary, Kongnoo et al. [27] reported a consistent increase of CO_2 adsorption with the increase of temperature over the range from 40-70°C, indicating the chemisorption of adsorbent-adsorbate interaction. From this finding, it could be deduced that the demarcation between physical and chemical adsorption of CO_2 by alkali impregnated activated carbons should occur at the temperature in the vicinity of 40°C.

Based on the above argument, the adsorption of CO_2 by the alkali-impregnated activated carbon in this work could be by physical interaction forces since the adsorption tests were conducted at 35°C. To check this further for the nature of adsorbent-adsorbate interaction forces, the equilibrium adsorption isotherms of CO_2 by AC2 and AC2-5 were measured at 0 and 20°C using a surface area analyzer (ASAP2020, Micromeritics, US). The results are shown in Fig. 13. It is noted that the amount of CO_2 adsorbed decreases with the increase of adsorption temperature for both types of activated carbon, indicating that the adsorption of CO_2 in the virgin activated carbon and activated carbon loaded with NaOH over this low temperature range does occur by physical interaction forces. It is further observed that the shape of CO_2 isotherms up to the relative pressure of 0.03 resembles that of N_2 isotherms in the low pressure range as shown in Fig. 2, suggesting that the adsorption of N_2 and CO_2 occur in small micropores of the activated carbon.

For physical adsorption, there are two diffusion mechanisms of an adsorbate inside the pores of an adsorbent, namely pore diffusion through the internal pore space as characterized by the pore diffusivity (D_p) and the surface diffusion as characterized by the surface diffusivity (D_s). The correlation of the effective diffusivity (D_e) with D_p and D_s is by the following equation [33],

$$D_e = \frac{\varepsilon_p D_p + (1-\varepsilon_p) K D_s}{\varepsilon_p + (1-\varepsilon_p) K} \tag{17}$$

The pore diffusivity (D_p) was first estimated from Eq. (18) and followed by the computation of D_s via Eq. (17), knowing the value of D_e and D_p.

$$D_p = [(1/D_{m,eff}) + (1/D_{k,eff})]^{-1} \tag{18}$$

where $D_{m,eff}$ = effective molecular diffusivity of $CO_2 = \varepsilon_p D_m / \tau$
$D_{k,eff}$ = effective Knudsen diffusivity = $\varepsilon_p D_k / \tau^2$
D_m = molecular diffusivity of CO_2
D_k = Knudsen diffusivity of CO_2
ε_p = particle porosity that is dependent on NaOH loading
τ = tortuosity factor = 5.75 for activated carbon [34]

Figure 14 shows typical variation of the three transport properties (D_e, D_p and D_s) for activated carbon AC1 as a function of NaOH loading. Both D_p and D_s have a general tendency to decrease with an increasing NaOH loading as expected. Also, it is seen that the surface diffusivity has a value close to that of the effective diffusivity and its value is about two orders of magnitude larger than that of the pore diffusivity. From these results, it can be concluded that surface diffusion is the major mechanism of CO_2 transport in coconut-shell activated carbon impregnated with NaOH, resulting from the large adsorbate concentration on the pore surface caused by the strong interaction of CO_2 molecules and NaOH active sites.

DOI:10.4186/ej.2019.23.4.29

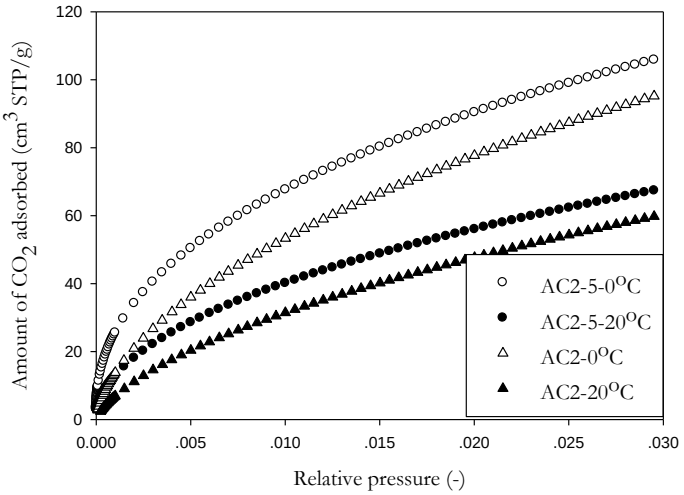

Fig. 13. CO_2 adsorption isotherms of the original activated carbon (AC2) and activated carbon impregnated with 5 wt% NaOH (AC2-5), showing the effect of temperature on the CO_2 adsorbed amounts (saturation vapour pressures of CO_2 at 0°C and 20°C are 3.5 MPa and 5.7 MPa, respectively).

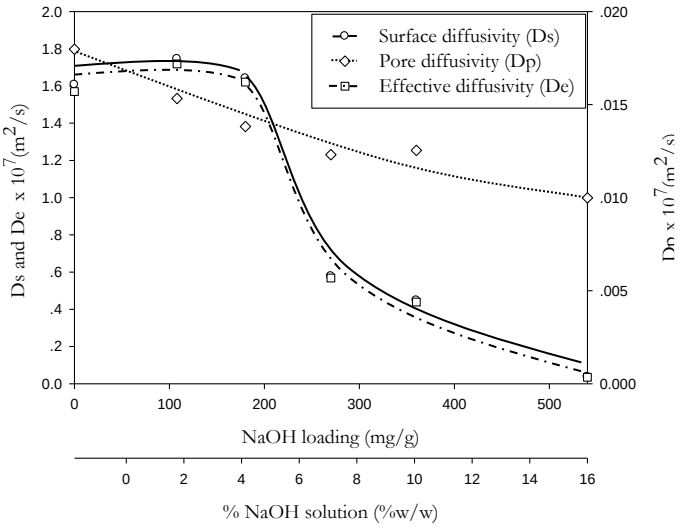

Fig. 14. Effect of NaOH loading on D_e, D_p and D_s for the diffusion of CO_2 in activated carbon AC1.

5. Conclusion

Fixed-bed adsorption of CO_2 by coconut-shell activated carbon impregnated with NaOH showed improved adsorption efficiency, as compared to the unmodified one. The adsorption dynamic parameters of the fixed bed, including the breakthrough time, the adsorbed capacity at the breakthrough time and the adsorbed capacity at equilibrium, were found to increase with the increase of NaOH loading and passed through a maximum value at approximately the same loading of 180 mg NaOH/g carbon. The maximum adsorbed capacity of CO_2 was 40% higher for the impregnated carbon, when compared with the original unmodified carbon. Activated carbon with larger pore volume and surface area can adsorb more CO_2 due to the larger number of available active sites. The pore blocking effect was hypothesized to be responsible for the fall of adsorbed capacity at a relatively high alkali loading. The breakthrough equation based on the LDF model, known as the Klinkenberg's equation, could predict the experimental breakthrough data very well up to the

exit concentration ratio (C/C_o) of 0.80. The model parameters (k_p and K) varied with NaOH loading in a similar fashion to that of the adsorption capacity. Further analysis of the breakthrough model's parameters showed that surface diffusion is the dominant transport mechanism of CO_2 inside the pores of activated carbon and the value of surface diffusivity was about two orders of magnitude larger than the pore diffusivity for the parallel diffusion of adsorbate through the pore space.

Acknowledgements

The support of this work in form of graduate scholarship to SN from Suranaree University of Technology is gratefully acknowledged.

References

[1] Y. C. Chiang and R. S. Juang, "Surface modification of carbonaceous materials for carbon dioxide adsorption: A review," *Journal of the Taiwan Institute of Chemical Engineers*, vol. 71, pp. 214-234, 2017.

[2] B. Metz, O. Davidson, H. de Coninck, M. Loos, and L. Meyes, *Intergovernmental Panel on Climate Change (IPCC). Special Report on Carbon Dioxide Capture and Storage*, Cambridge, UK and New York, USA: Cambridge University Press, 2005.

[3] Science Daily. (2018). *Carbon Dioxide Emissions from Power Plants Rated Worldwide* [Online]. Available: www.sciencedaily.com/releases/2007/11/071114163448.htm

[4] D. Y. C. Leung, G. Caramanna, and M. M. Marotq-Vales, "An overview of current status of carbon dioxide capture and storage technologies," *Renewable and Sustainable Energy Reviews*, vol. 39, pp. 426-443, 2014.

[5] N. A. Rashidi and S. Yusup, "An overview of activated carbon utilization for the post-combustion carbon dioxide capture," *Journal of CO_2 utilization*, vol. 13, pp. 1-16, 2016.

[6] A. L. Chaffee, G. P. Knowles, Z. Liang, I. Zhang, P. Xiao, and P. A. Webley, "CO_2 capture by adsorption: Materials and process development," *International Journal of Greenhouse Gas Control*, vol. 1, pp. 11-18, 2007.

[7] A. L. Yaumi, M. Z. Abu Bakar, and B. H. Hameed, "Melamine-nitrogenated mesoporous activated carbon derived from rice husk for carbon dioxide adsorption in fixed-bed," *Energy*, vol. 155, pp. 46-55, 2018.

[8] A. E. Creamer, B. Gao, and S. Wang, "Carbon dioxide capture using various metal oxyhydroxide-biochar composites," *Chemical Engineering Journal*, vol. 283, pp. 826-832, 2016.

[9] J. Singh, H. Bhunia, and S. Bagu, "Synthesis of porous carbon monolith adsorbents for carbon dioxide capture: Breakthrough adsorption study," *Journal of the Taiwan Institute of Chemical Engineers*, vol. 89, pp. 140-150, 2018.

[10] O. Boujibar, A. Souikny, F. Ghamouss, O. Achak, M. Dahbi, and T. Chafik, "CO_2 capture using N-containing nanoporous activated carbon obtained from argan fruit shell," *Journal of Environmental Chemical Engineering*, vol. 6, pp. 1995-2002, 2018.

[11] N. A. Rashidi, S. Yusup, and A. Borhan, "Development of novel low-cost activated carbon for carbon dioxide capture," *International Journal of Chemical Engineering and Applications*, vol. 5, pp. 90-94, 2014.

[12] A. S. Ello, L. K. C. de Souza, A. Trokourey, and M. Jaroniec, "Coconut shell-based microporous carbons for CO_2 capture," *Microporous and Mesoporous Materials*, vol. 180, pp. 280-283, 2013.

[13] E. David and J. Kopac, "Activated carbon derived from residual biomass pyrolysis and their CO_2 adsorption study," *Journal of Analytical and Applied Pyrolysis*, vol. 110, pp. 322-332, 2014.

[14] S. Shahkarami, R. Azargohar, A. K. Dalai, and J. Soltan, "Breakthrough CO_2 adsorption in bio-based activated carbon," *Journal of Environmental Science*, vol. 34, pp. 68-76, 2015.

[15] B. S. Caglayan and A. E. Aksoylu, "CO_2 adsorption on chemically modified activated carbon," *Journal of Hazardous Materials*, vol. 252-253, pp. 19-28, 2013.

[16] D. Das and B. C. Meikap, "Comparison of adsorption capacity of mono-ethanolamine and di-ehanolamine impregnated activated carbon in a multi-stage fluidized bed reactor for carbon-dioxide capture," *Fuel*, vol. 224, pp. 47-56, 2018.

[17] Z. Chen, S. Deng, H. Wei, B. Wang, J. Huang, and G. Yu, "Activated carbons and amine-modified materials for carbon dioxide capture—A review," *Frontiers of Environmental Science & Engineering*, vol. 7, pp. 326-340, 2013.

[18] Y. L. Tan, Md. A. Islam, M. Asif, and B. H. Hameed, "Adsorption of carbon dioxide by sodium hydroxide modified granular coconut shell activated carbon in a fixed bed," *Energy*, vol. 77, pp. 926-931, 2014.
[19] I. D. Seader and E. J. Henley, *Separation Process Principles*. John Wiley & Sons, 1998, ch. 15, p. 834.
[20] R. T. Yang, *Gas Separation by Adsorption Process*. Imperial College Press, 1997, ch. 4, p. 125.
[21] D. M. Ruthven, *Principles of Adsorption and Adsorption Process*. John Wiley & Sons, 1984, ch. 8, p. 236
[22] N. Wakao and T. Funazkri, "Effect of fluid dispersion coefficients on particle-to-fluid mass transfer coefficients in packed beds: Correlation of Sherwood numbers," *Chemical Engineering Science*, vol. 33, pp. 1375-1391, 1978.
[23] R. B. Bird, W. E. Stewart, and E. N. Lightfoot, *Transport Phenomena*. John Wiley & Sons, 1960, ch. 16, p. 510.
[24] D. D. Do, *Adsorption Analysis: Equilibria and Kinetics*. Imperial College Press, 1998, ch. 3, p. 84.
[25] F. Rouguerol, J. Rouguerol, and K. Sing, *Adsorption by Powders and Porous Solids*. Academic Press, 1999, ch. 6, p. 176.
[26] K. S. W. Sing, D. H. Everett, R. A. W. Haul, L. Moscou, R. A. Pierotti, J. Rouqueral, and T. Siemieniewska, "Reporting physisorption data for gas/solid systems with special reference to the determination of surface area and porosity," *Pure & Appl. Chem.*, vol. 57, pp. 603-619, 1985.
[27] A. Kongnoo, P. Intharapat, P. Worathanakul, and C. Phalakornkule, "Diethanol amine impregnated palm shell activated carbon for CO_2 adsorption at elevated temperature," *Journal of Environmental Chemical Engineering*, vol. 4, pp. 73-81, 2016.
[28] M. Auta, M. Umaru, M. D. Yahya, O. D. Adeniyi, I. M. Aris, and B. Suleiman, "Diethanilamine functionalized waste tea activated carbon for CO_2 adsorption," in *International Conference on Chemical, Environment and Biological Science (CEBS-2015)*, Dubai (UAE), 2015.
[29] M. Auta and B. H. Hameed, "Adsorption of carbon dioxide by diethanolamine activated alumina beads in a fixed bed," *Chemical Engineering Journal*, vol. 253, pp. 350-355, 2014.
[30] C. S. Lee, Y. L. Ong, M. K. Aroua, and W. M. A. W. Daud, "Impregnation of palm shell-based activated carbon with sterically hindered amines for CO_2 adsorption," *Chemical Engineering Journal*, vol. 219, pp. 558-564, 2013.
[31] L. Ma, R. Bai, G. Hu, R. Chen, X. Hu, W. Dai, and H. F. M. Dacosta, "Capturing CO_2 with amine-impregnated titanium oxides," *Energy & Fuels*, vol. 27, pp. 5433-5439, 2013.
[32] M. Auta, N. D. A. Darbis, A. T. M. Din, and B. H. Hameed, "Fixed-bed column adsorption of carbon dioxide by sodium hydroxide modified activated carbon," *Chemical Engineering Journal*, vol. 233, pp. 80-87, 2013.
[33] C. Tien, *Adsorption Calculations and Modeling*. Butterworth-Heinemann, 1994, ch. 6, p. 88.
[34] E. Costa, G. Calleja, and F. Domingo, "Adsorption of gaseous hydrocarbons on activated carbon: Characteristic kinetic curve," *AIChE Journal*, vol. 31, pp. 982-987, 1985.